Physica A 592 (2022) 126734

Contents lists available at ScienceDirect

Physica A

journal homepage: www.elsevier.com/locate/physa

A dynamic physical-distancing model to evaluate spatial measures for prevention of Covid-19 spread ☆

Tianyi Xiao [a], Tong Mu [a], Sunle Shen [a], Yiming Song [a], Shufan Yang [a], Jie He [a,b,*]

[a] School of Architecture, Tianjin University, Tianjin, China
[b] School of Architecture, Harbin Institute of Technology (Shenzhen), Shenzhen, Guangdong Province, China

ARTICLE INFO

Article history:
Received 13 August 2021
Received in revised form 7 November 2021
Available online 25 December 2021

Keywords:
Physical distancing
Infection dynamics
Pedestrian dynamics
Space design
Self-organisation phenomena

ABSTRACT

Motivated by the global pandemic of COVID-19, this study investigates the spatial factors influencing physical distancing, and how these affect the transmission of the SARS-CoV-2 virus, by integrating pedestrian dynamics with a modified susceptible–exposed–infectious model. Contacts between infected and susceptible pedestrians are examined by determining physical-distancing pedestrian dynamics in three types of spaces, and used to estimate the proportion of newly infected pedestrians in these spaces. Desired behaviour for physical distancing can be observed from simulation results, and aggregated simulation findings reveal that certain layouts enable physical distancing to reduce the transmission of SARS-CoV-2. We also provide policymakers with several design guidelines on how to proactively design more effective and resilient space layouts in the context of pandemics to keep low transmission risks while maintaining a high pedestrian volume. This approach has enormous application potential for other infectious-disease transmission and space assessments.

1. Introduction

As of May 2021, there had been 160 million confirmed cases of coronavirus disease 19 (COVID-19), and almost 3.4 million deaths, across 230 countries and regions worldwide [1]. Research has shown that frequent intra-metropolitan travel and social, sports, religious, and cultural gatherings in transportation hubs, stadiums, places of worship, and nightclubs are essential drivers of the transmission of severe acute respiratory syndrome coronavirus 2 (SARS-CoV-2), which causes COVID-19 [2,3]. Thus, many countries that have experienced increasingly severe outbreaks have implemented population-level physical-distancing measures and movement restrictions, such as business closures, community lockdowns, and the cancellation of large-scale public gatherings, which have slowed the transmission of SARS-CoV-2 [4]. However, the effects of spatial configurations on physical distancing-based attempts to prevent SARS-CoV-2 transmission remain unclear [5,6]. Specifically, despite the consensus that physical distance should be maintained between people [6], there are few data and even less agreement on what kinds of spatial layouts are needed and what proportion of physical isolation is required on a micro-scale.

To address this research gap, we propose a systematic simulation-based approach to effectively capture the mechanics of spatial factors influencing the ability of physical distancing to prevent SARS-CoV-2 transmission and to model the

☆ This research was supported by Open Projects Fund of Key Laboratory of Ecology and Energy-Saving Study of Dense Habitat (Tongji University), Ministry of Education, China, Grant No. 2020030101.

* Correspondence to: School of Architecture, Harbin Institute of Technology (Shenzhen), University Town of Shenzhen, Nanshan District, Shenzhen, Guangdong Province, 518055, China.
E-mail address: hejie2021@hit.edu.cn (J. He).

https://doi.org/10.1016/j.physa.2021.126734

probability of transmission in various spatial configurations. First, based on the social force model (SFM), we develop algorithms for physical-distancing dynamics in terms of exploratory collective human interactions and socio-psychological exclusion. Second, we integrate pedestrian dynamics with a modified susceptible (S) – exposed (E) – infectious (I) (SEI) model, which generates insights into how spaces can be better managed to reduce the transmission of SARS-CoV-2.

2. Literature review

Investigating the mechanism of interpersonal SARS-CoV-2 transmission is a complex undertaking that demands close collaboration between various research fields. Previous studies in this area can be categorised in terms of their multidisciplinary features into two main topics: epidemiology and pedestrian dynamics. These studies are reviewed below.

2.1. Epidemiology

Deterministic modelling [7] and stochastic modelling [8] are widely used to mathematically model the spread of infections. An example of such models is SIR models, which classify individuals as S, I, or removed (R) [7]. However, such models regard the size of a population as constant and thus fail to account for the fact that the volumes of pedestrians in real-life public spaces are variable and dynamic. In addition, these models do not consider mobility processes and human interactions in pedestrian crowds [7], despite these being essential to the transmission of infection, and thus do not predict actual transmission. Consequently, these models can rarely reveal by whom and when an individual was infected [9] and where the infection occurred.

Spatial stochastic epidemic models, e.g., the global epidemic and mobility model [10], and a data-driven mobility model [11] describe human mobility as a commuting network of interacting communities. These models focus on spatiotemporal patterns of intercontinental and urban commuting, thereby describing the spread of infection through continental commuting networks or global airline-transportation networks. Consequently, such models are used to develop macroscopic approaches to managing commuting to minimise the spread of infection during a public health emergency. However, relatively little effort has been devoted to examining microscopic interactions between pedestrians, and thus the effectiveness of community-scale infection-prevention measures is unclear.

2.2. Pedestrian dynamics

Knowledge of human mobility and connectivity patterns can yield key insights to aid the development of efficacious crowd-management and pandemic-response procedures [12]. An increasing number of pedestrian dynamics models have been developed over the past decades, such as (1) magnetic model [13], which regards pedestrians or obstacles as positive poles and destinations as negative poles; (2) cellular automaton model [14], which consists of pedestrians with discrete states, and the pedestrians evolve in discrete time steps according to definite rules, (3) fluid-dynamic model [15], which is similar to the equations for ordinary fluids, but it is coupled equations for several fluids and contain some additional terms that are characteristic for pedestrian fluids. In addition, the SFM [15] is a typical microscopic model, which can separately model individuals' trajectories. Since the work of Helbing and Molnár [15], SFM has been used in a variety of studies, such as studies on emergency evacuation [16], facility design [16], collective phenomena [17], and route optimisation [18]. However, better algorithms are required for modelling pedestrian dynamics using the SFM, as many subproblems have yet to be adequately addressed, such as oscillation elimination [19], systems equilibria [20], collision sensitivity [21], calibration of model parameters [16], and boundary detection [22], particularly for new interaction rules such as physical distancing.

Motivated by the COVID-19 pandemic, an increasing amount of studies have taken physical distancing into account experimentally or numerically in pedestrian dynamics. Daniel R et al. [23] measured events of physical-distancing less than 2 m and their duration by pedestrian simulations in an ideal supermarket to investigate the effect of customer number on physical distancing. They suggested increasing the number of checkout points and decreasing the clients' checkout time to maintain the physical distancing. Echeverría et al. [24] demonstrated pedestrian density, walking speed, and prescribed safety distance are three significant factors when people walk on physical distancing within relatively dense crowds by controlled laboratory experiments. Caspar et al. [25] developed a scalable algorithm to analyse the encounter patterns of distance-time in a crowd in real-time. This method was based on data from commercial pedestrian tracking sensors to identify social groups and monitor physical-distancing, which provided technical support for people's physical-distancing management in public spaces. Christina et al. [26] simulated the physical-distancing of 1.5 m and 2.0 m to propose new parameter values for personal space in the Optimal Steps Model (OSM), enabling developers to conveniently conduct relevant studies on social distance. These studies have put forward some new technologies and management methods to physical distancing, but less consideration of the epidemic transmission in crowd movements.

Other researchers proposed spatial optimisation strategies reduce the spread of infection. These researches provided scientific guidance for space design criteria and pedestrian management strategies by analysing individual trajectories and intervals between pedestrians in a busy and congested environment. For example, Namilae and colleagues [27] proposed a SFM-based multiscale model to study Ebola transmission within aeroplanes, and used the results from the model to evaluate the infection dynamics of various boarding and deplaning policies aimed at preventing the geospatial spread of

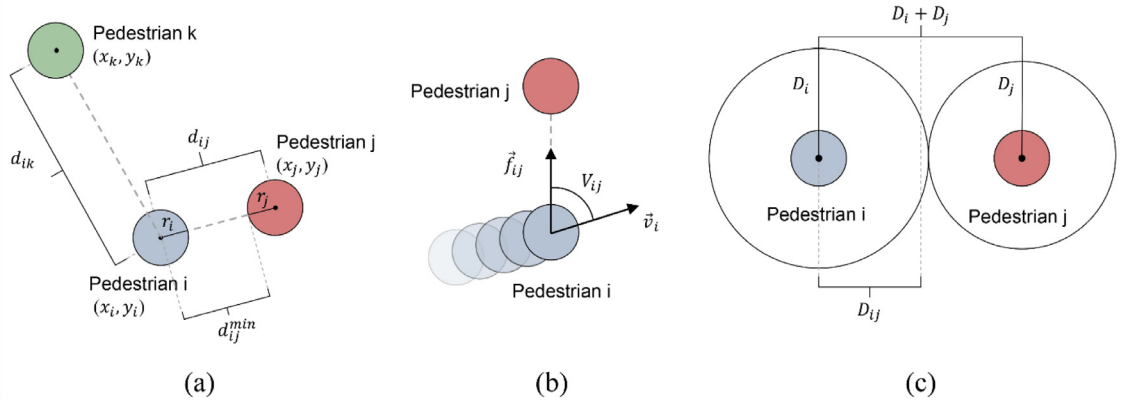

Fig. 1. (a) Minimum distance d_{ij}^{min} (b) Visual angle V_{ij} (c) Average prevention sphere D_{ij}.

infectious diseases. Derjany et al. [28] formulated a stochastic infection-spread model that describes the propagation of disease among large groups of people, and a SFM-based pedestrian movement model to simulate realistic human queuing behaviour. Their results revealed that queues comprising short aisles with rope separators were significantly associated with a lower spread of infection. Sun et al. [29] used accurate student-contact data and a continuous infection model to calculate effective distances for investigating the transmission of SARS-CoV-2 in a school in three types of area-isolation scenarios. Their results suggested that digital contact tracing was similarly effective in mitigating SARS-CoV-2 transmission as fully enclosed school management.

The above-mentioned studies considered people's movement when conventional inter-personal distances are maintained. However, little attention has been paid to the effects of physical-distancing dynamics on infection transmission in these contexts. Moreover, many studies on infection transmission have been based on binomial distribution estimations, which do not accurately model airborne transmission via aerosols and droplets. Furthermore, research has tended to focus on examining the trajectories of pedestrians rather than pedestrian self-organisation phenomena, despite the fact that such phenomena may lead to many infection events.

As there are limitations to the use of the original SFM for describing pedestrian flows under physical-distancing conditions, we first modify the original SFM equations by applying a neighbour-dependent self-slowing mechanism and epidemic-prevention psychological repulsion, which prevent a simulated pedestrian from coming into close contact with other pedestrians. This modified model can determine the trajectories of S and I pedestrians in crowds under physical-distancing conditions. These trajectories are integrated into a physical distance model (PDM), which serves as a computational platform to simulate the fine-scale transmission of SARS-CoV-2-like infections. To fully consider the effect of pedestrian mobility processes on transmission dynamics, we develop an infection-assessment module that has four main parameters: breathing cycle, the probability of infection transmission, the strength of infectivity, and contact radius. We use this model to evaluate the interactive infection and health-status conversion of pedestrians in various space configurations, and to simulate the effect of tuneable physical-distancing ratios on pandemic spread.

3. Methods

3.1. Definition of influential factors

Many factors imperceptibly influence a pedestrian's behavioural decisions on physical distancing for preventing the transmission of infection; these include his/her distance from others, viewshed, and psychology. Thus, we use three significant factors to describe pedestrian movement more precisely: minimum distance, visual angle, and average prevention sphere. Describing pedestrians P_i as disks of radius r_i and position of the centre of mass (x_i, y_i), the schematic diagrams of these factors are shown in Fig. 1.

Minimum distance d_{ij}^{min}. A pedestrian moving and performing physical distancing is most affected by the nearest person in his/her field of vision. To model this scenario, we introduce d_{ij}^{min}, which is defined as

$$d_{ij}^{min} = \min\{d_{ij} - r_j; j \neq i\} \tag{1}$$

where $d_{ij} = \sqrt{(x_j - x_i)^2 + (y_j - y_i)^2}$, which is the distance between the position of P_i and P_j.

Visual angle V_{ij}. According to an experience-driven mindset, pedestrians generally notice pedestrians in front of them rather than those behind them [16]. Thus, we add V_{ij}, which shows the extent of an observer's eye looking at frontally,

to enhance the validity of our simulation with respect to visual physiology or psychological perception data. V_{ij} between a pair of pedestrians is given by

$$V_{ij} = \arccos\left(\frac{\vec{v}_i \cdot \vec{n}_{ij}}{\|\vec{v}_i\| \, \|\vec{n}_{ij}\|}\right) \tag{2}$$

Where $\vec{v}_i$ is the velocity of P_i, and $\vec{n}_{ij} = \frac{((x_j,y_j)-(x_i,y_i))}{d_{ij}}$, which is the normalised vector pointing from P_j to P_i. V_{ij} denotes the included angle between the walking direction of P_i and $\vec{n}_{ij}$.

Average prevention sphere D_{ij}. This factor reflects the tendency of a pedestrian to keep a distance from others, where D_i is zero if P_i does not have an awareness of infection prevention measures, and is otherwise a pedestrian's desired physical distance. $D_{ij} = \left(D_i + D_j\right)/2$ is the average size of the prevention sphere between P_i and P_j.

3.2. Physical-distancing pedestrian dynamics

We create a many-particle system in which each pedestrian is represented separately as an agent or particle with individual properties, namely mass, desired speed, desired distance between others, view angle, and wayfinding behaviour. Each particle's acceleration is controlled by its desired speed and the influence of other particles, as in the SFM [15]. The corresponding expression of the change in velocity of pedestrian (or particle) P_i with mass m_i and who is performing physical distancing ($D_i > 0$) is then given by

$$\frac{d\vec{v}_i}{dt} = \vec{f}_i^{(self)} + \frac{1}{m_i}\vec{f}_i^{(others)} \tag{3}$$

where $\vec{f}_i^{(others)}$ is the total force due to other particles, and $\vec{f}_i^{(self)}$ represents a self-propelled force that makes a particle attempt to move to the terminus at its desired speed, and can thus be regarded as a driving term.

As mentioned above, distance and V_{ij} are two crucial factors in the movement of a pedestrian who performs physical distancing. Firstly, as particles should move at a certain distance from a particle in front of them, a self-slowing mechanism is introduced when the particle in front contacts the average prevention sphere; this involves the desired speed of P_i decreasing towards zero until the particle in front is no longer contacting the prevention sphere. Secondly, the human horizontal binocular view-angle without head movement is 124° (0.68π) [30], which can be taken as the criterion for deceleration detection. The typical structure of $\vec{f}_i^{(self)}$ is defined by

$$\vec{f}_i^{(self)} = \begin{cases} \frac{\varphi v_i^0 \vec{e}_i^0 - \vec{v}_i}{\tau}\left[1 - \varphi\left(\frac{D_{ij}}{d_{ij}^{min}}\right)^2\right], \; V_{ij} \le 0.34\pi; \; \varphi = \begin{cases} 0, & D_{ij} \ge d_{ij}^{min} \\ 1, & D_{ij} < d_{ij}^{min} \end{cases} \\ \frac{1}{\tau}(v_i^0 \vec{e}_i^0 - \vec{v}_i), \; V_{ij} > 0.34\pi \end{cases} \tag{4}$$

where P_j is the nearest particle to P_i. v_i^0 is the desired speed, $\vec{e}_i^0$ is the desired direction, and τ is the relaxation time within which $\vec{v}_i$ achieves $v_i^0\vec{e}_i^0$. φ is the cut-off distance constant that equals 0 if the average prevention sphere is occupied by P_j, and is otherwise equal to 1. Thus the desired velocity of P_i reduces to zero when $\varphi = 0$, and the self-propelled force of P_i decreases with proximity to P_j when $\varphi = 1$. 0.34π is the maximum radian up to which the self-slowing mechanism should not be triggered in simulation because P_j is out of view and the calculation method turns to the original SFM acceleration force [31].

Under physical-distancing conditions, particles maintain a physical distance from each other to prevent the transmission of infection. The closer one particle is to another given particle, the more vigilance the other particle arouses in the given particle. We describe this psychological effect using a two-part repulsive interaction force: the first part is the prevention force of the nearest particle (P_j) and the second part is the physical force of surrounding particles aside from P_j. Thus, we have

$$\vec{f}_i^{(others)} = \begin{cases} A_i^p\left[\frac{D_{ij}-d_{ij}^{min}}{D_{ij}}\right]\vec{n}_{ij} + \sum_{k(\neq i,j)} A_i^1 exp\left[\frac{r_{ik}-d_{ik}}{B_i^1}\right]\vec{n}_{ik}, D_{ij} > d_{ij}^{min} \\ \sum_{k(\neq i)} A_i^1 exp\left[\frac{r_{ik}-d_{ik}}{B_i^1}\right]\vec{n}_{ik}, D_{ij} \le d_{ij}^{min} \end{cases} \tag{5}$$

where A_i^p, A_i^1, and B_i^1 are constants: the first two can be interpreted as the strength of the interaction between the private sphere and the prevention sphere, and the third determines the range of this interaction of the private sphere. $\vec{n}_{ik}$ have the same calculation structure of $\vec{n}_{ij}$, which is the normalised vector pointing from P_k to P_i. d_{ik} is the distance between positions of P_i and P_k, and $r_{ik} = r_i + r_k$ is the sum of the radii. Further, D_{ij} is the critical distance between P_i and P_j in a line at which the rear pedestrian bear back. Eq. (5) ensures that the repulsive force between pedestrians is increased when a pedestrian lies inside the prevention sphere of another particle. To be more specific, the first term in Eq. (5) no longer applies and is considered to be zero when the distance between them exceeds the prevention sphere, and thus repulsive interactions with neighbours adopt the second term in Eq. (5) regardless of whether they are the nearest one.

Table 1
Physical attributes of male and female adults in the Chinese population.

Parameter	Definition	Male range	Female range	Reference
r_i	Half shoulder-width	191–243 mm	173–229 mm	[33]
m_i	Mass	44–83 kg	38–74 kg	[33]
v_i^0	Desired walking speed	1.30–1.56 m/s	1.20-1.46 m/s	[32]

Table 2
Parameters and data ranges used in the physical-distancing model.

Parameter	Definition	Estimate	Reference
A_i^1	Private sphere interaction strength	2×10^3 N	[34]
B_i^1	Interaction range	0.08 m	[34]
D_i	Desired physical distance	1 m	[35,36]
A_i^p	Prevention sphere interaction strength	20 N	
τ	Relaxation time	1 s	[16]

Pedestrian physical attributes are essential parameters in the model, and include desired walking speed v_i^0, mass m_i, and shoulder-width r_i, in addition to psychological attributes, such as physical distance and private sphere. Knoblauch et al. quantified the walking speed range of pedestrians [32], while mass and shoulder width can be found in the National Standard Human Dimensions of Chinese Adults [33]. Other parameters are private sphere interaction strength (A_i^1) and interaction range (B_i^1), which are the same as the corresponding SFM parameters. However, a final parameter – prevention sphere interaction strength (A_i^p) – is difficult to measure directly, and we estimate it by comparing the outcomes of simulations of the average distance between pedestrians during movement with pedestrians' desired distance from each other. Tables 1 and 2 list the details of these pedestrian dynamic parameters.

3.3. Infection assessment

Exhaled aerosols are three-dimensional, making it challenging to perform complete spatial measurements of their distribution. Therefore, we treat exhaled aerosols as two-dimensional for the transmission calculations. Moreover, as we simulate possible short-term SARS-CoV-2 transmission scenarios, it is not essential to simulate all infection-transmission scenarios. Instead, we quantify the exposure possibility. Accordingly, within a crowd, we use a compartmental representation of SARS-CoV-2 transmission possibility, consisting of I, E (infected but not yet infectious), and S pedestrians. An S pedestrian can inhale SARS-CoV-2 particles through contact with an I pedestrian, and thus become an E pedestrian [4].

We calculate the duration of contact between an I pedestrian and an S pedestrian by using the infection radius and infectivity of the I pedestrian, to determine whether the S pedestrian becomes an E pedestrian. We denote by $\{p_1, \ldots, p_n\}$ the pedestrians in population N, such that $N(t) = I(t) + S(t) + E(t)$ at time t. We create potential transmission links between all S and I pedestrians. Formally, these links are written as $L = \left\{\overline{P_i P_s} \mid P_i \in I \wedge P_s \in S\right\}$.

We denote continuous time by $t \in [0, T]$, with 0 and T denoting the beginning and the end of a breathing cycle. At time $t \in [0, T]$, C_n is the quanta of infectious particles in any cross-section of aerosols that a pedestrian contacts in a breathing cycle. Then, the formulations for every link $\overline{P_i P_s}$ take the form

$$C_n = C_0 \int_0^T f\left(\vec{r}_i(t) - \vec{r}_s(t)\right) dt \tag{6}$$

$$f\left(\vec{r}_i(t) - \vec{r}_s(t)\right) = \frac{1}{\pi R_C^2} exp\left[-\left(\frac{\left\|\vec{r}_i(t) - \vec{r}_s(t)\right\|}{R_C}\right)^2\right] \tag{7}$$

where $\vec{r}_i(t)$ and $\vec{r}_s(t)$ are the positions of P_i and P_s, respectively, R_C is the radius of transmission of SARS-CoV-2, and C_0 is the maximum initial concentration of infectious particles in aerosols produced by infected pedestrians during breathing, speaking, coughing, and sneezing [37]. Eq. (7) is a Gaussian distance-dependent weight function [37–39] describing the distribution of SARS-CoV-2 particle-shedding in terms of the distance between I and S pedestrians. We assume a distance-dependent spatial variation in the concentration of infected aerosols [37], such that the concentration of infectious particles increases with proximity to their source. Then, with respect to C_n, the probability of infection is given by Wells–Riley equation [40] $p = 1 - e^{-\gamma C_n}$ with γ being an adjustment coefficient. If transmission does not occur, C_n is reset and the subsequent respiration-cycle assessment begins.

The four parameters in the infection-assessment module are T, C_0, R_C, and γ. Research shows that an S person can inhale infectious particles within 4 s, and thus we set T to 4 s [41]. C_0 is represented by the SARS-CoV-2 particle-shedding probability [42] defined as ommllog10 virus copies per sample, which begins more than a week before symptom onset and declines quickly within 7 days after onset [43] (see Fig. 2(a)). To decrease the computational load, we set a constant

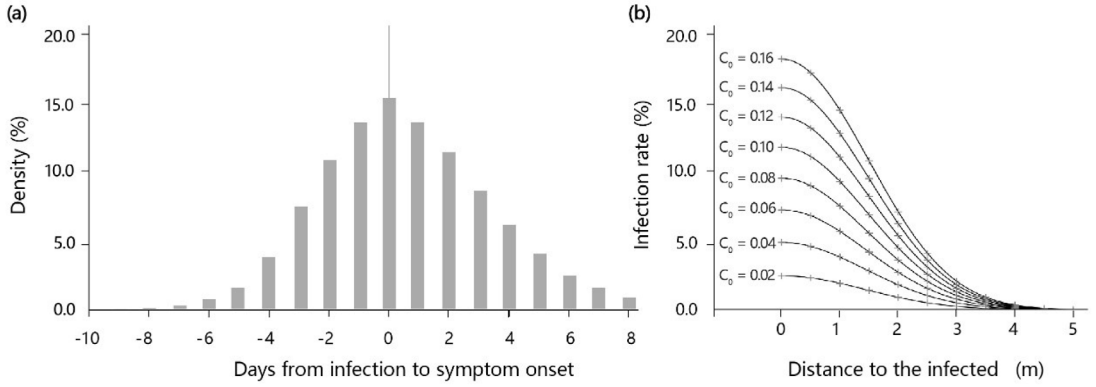

Fig. 2. (a) Inferred the distribution of C_0, modified by data from Ref. [43]. (b) Infection rate profiles for various values of C_0, with $\gamma = 4$, $R_C = 2$, and $T = 4$.

$C_0 = 0.16$. In previous research [44,45], SARS-CoV-2-bearing aerosols were detected in air samplers 2 m away from patients, and thus we set $R_C = 2$ m. However, smaller droplets and aerosols can remain airborne for a long time, contributing to disease transmission over longer distances [46]. Hence, there is an infection risk beyond the radius, although the probability of infection decreases drastically at greater distances (see Fig. 2(b)). Moreover, because virus transmission is unexpected and fatal, which excludes real-life experiments, we could not find relevant data on infectivity strength to test our model quantitatively. Therefore, we give a reasonable estimate value of $\gamma = 4$, which measures the strength of infectivity.

4. Results

4.1. Baseline configurations

Three types of typical public-space scenarios are investigated: (1) the evacuation of passengers from a room with narrow exits; (2) bidirectional pedestrian streams in a linear corridor, with and without obstacles or railing separators; and (3) the movement of pedestrians in winding queues. Due to the inherent uncertainty in human motion and the stochasticity of the infection-assessment model, and the fact that the positions of infected pedestrians are unpredictable, we simulate the pedestrian dynamics of each experimental scenario via thousands of independently repeated experiments that use the same parameters. We removed outlier results, defined as cases more than 1.5 times the interquartile range from the median [47]. Then the validity and general mechanism of the experimental results are determined.

4.2. Performance evaluation measures

The average infection percentage (P_{ai}) and average contact time (T_{ac}) are two essential measures we use to compare the reduction in transmission due to various space-management strategies, and thereby determine which strategy is the best. P_{ai} represents what percentage of people in the population is infected in the simulations. The contact estimating range is based on the desired physical distance of pedestrians, so T_{ac} represents the average time of people surrounding a pedestrian who are closer to the pedestrian than D_{ij} per breathing cycle. T_{ac} of a pedestrian is calculated by summing all of the pedestrian data in all simulations and dividing this sum by the number of simulations, and the histograms of T_{ac} are normalised between 0 and 1 by dividing the data by T.

Furthermore, we account for the effect of variations in the physical-distancing rate (R_{pd}), which represents how many pedestrians in the population try to repel each other and therefore take into account the physical-distance term in Eq. (5) in the simulation while otherwise follow the original SFM interaction forces with other pedestrians [34]. We vary the R_{pd} from 0% of population (as in the SFM) and 100% of population (in the fully applied PDM), and plot the corresponding average distributions of newly infection-transmission pedestrians (D_{ai}) for various extents of physical distancing. D_{ai} over the probability range is obtained by integrating the pedestrian trajectories and contact data into the infection assessment model. Moreover, the trajectory of pedestrians during simulations is collected to calculate the track density raster using a kernel function in ArcGIS 10.7 [48].

4.3. Results of closed-room simulation

We model a 15 m $\times$ 15 m room with a 1.5-m-wide exit, similar to the dimensions of standard library reading-rooms. As several spatial configurations, such as various numbers or widths of exits, have been investigated in earlier studies

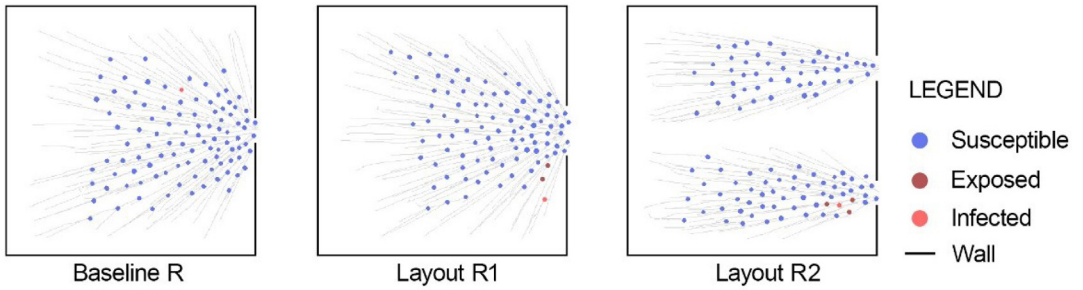

Fig. 3. Snapshot of three configurations of closed-room simulations (simulation: 8 s; $R_{pd} = 100\%$).

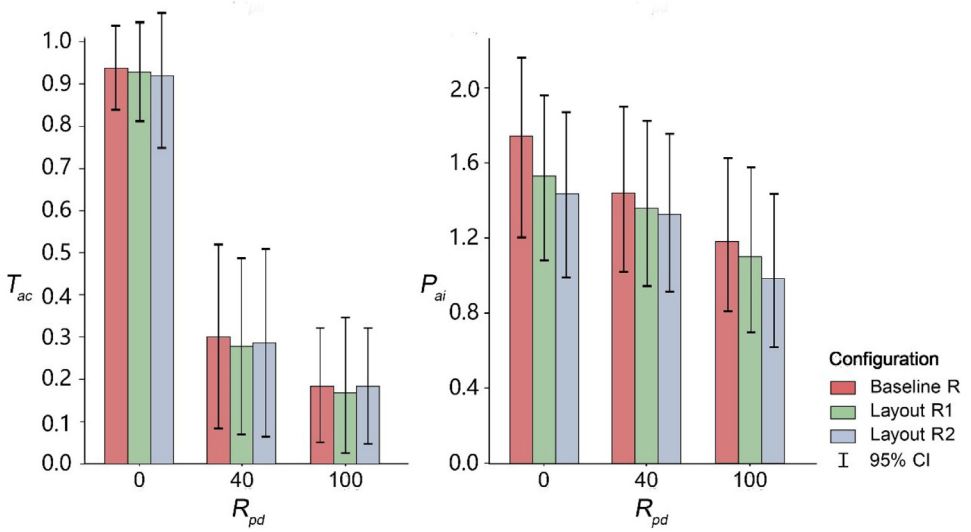

Fig. 4. Profiles of T_{ac} and P_{ai} for various closed-room configurations and R_{pd}.

of evacuation scenarios [49], we examine and compare the effects of three spatial configurations on the transmission of infection during evacuation, as shown in Fig. 3. Specifically, the room shape and area are constant and the configurations are Baseline R (one 1.5-m-wide exit), Layout R1 (one 3-m-wide exit), and Layout R2 (two 1.5-m-wide exits). We randomly distribute 120 pedestrians in three configurations, with 1 pedestrian initially infected, to simulate the effects of physical distancing on evacuation and on infection transmission. The two stop-conditions for the simulation are a simulation duration exceeding 60 s, and the timepoint at which all pedestrians have evacuated.

Integration of the simulation data (Fig. 4) shows that the Layout R2 configuration is the best with the lowest P_{ai}, followed by the Layout R1 configuration, while the Baseline R configuration is the worst. A negative correlation can be seen between P_{ai} and R_{pd} in three configurations, and T_{ac} drops dramatically as R_{pd} increases, while the width and number of exits affect slightly. Therefore, in contrast to the physical layout of the room, it is more efficient and effective to increase R_{pd} through spatial organisation policies, to prevent the transmission of the SARS-CoV-19 virus.

Moreover, the average time for complete evacuation for the Baseline R configuration is 28.8 s, whereas those for the Layout R1 and R2 configurations are 25.1 s and 26.84 s, respectively. This means that Layout R1 and R2 enable more efficient evacuation and less gathering and interpersonal encounter time around the exits than the Baseline R configuration. This is because the single exit of the Baseline R configuration is too narrow to evacuate a widely distributed crowd as R_{pd} increases, leading to congestion at this exit. Consequently, there is a longer T_{ac} and P_{ai} in the Baseline R configuration than in Layout R1 and R2.

As shown in Fig. 5, the most common result is the infection of zero to two people during evacuation, but severe infection events do occur, in which up to nine susceptible pedestrians are infected. Moreover, The Layout R2 configuration has the lowest trajectory density, which accounts for its lower probability of large-scale transmission.

Pedestrian arching occurs at the exits in the Baseline R and Layout R1 configurations, because pedestrians from all directions follow the shortest path to the exits. However, this arching is distinct from that observed in the SFM [34], as the distance between pedestrians in the outer arching is greater than the distance between them in the inner arching. Thus, although preventive forces and slowing mechanisms are operative, pedestrians at the rear continually exert pressure

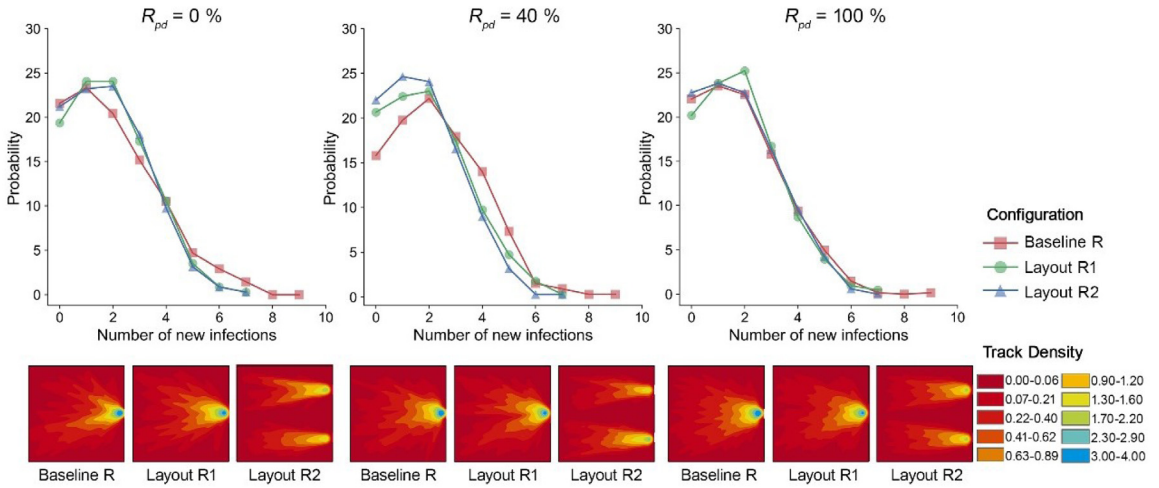

Fig. 5. Track densities and D_{ai} profiles of closed-room simulations for various R_{pd}.

on pedestrians at the front, generating an uneven density as time progresses. Consequently, although the trajectory distribution of pedestrians in the inner arching slightly broadens as R_{pd} increases, this does not result in a significant reduction in the probability of infection because of the space limitations and the concentration of pedestrians at the exits.

4.4. Results of the corridor simulation

We take a typical underground passage as a reference, and select a 6 m wide and 30 m long corridor for simulation. Bidirectional pedestrians enter the simulation area on both sides. Several studies have reported that oppositely moving pedestrians cause mutual obstruction [17,50], which can be effectively addressed by the placement of obstacles [16,51]. To verify whether this strategy is effective under conditions of physical distancing, we add a series of $0.5m \times 0.5m$ columns in the middle of the corridor. We also conduct a comparative experiment using impassable railings to determine whether the permeability of an interface between pedestrians moving in opposite directions affects the transmission of infection. To be more specific, the Layout C1 configuration comprises a corridor divided by impassable railings, whereas the separator of Layout C2 configuration is a series of columns. In the three corridor configurations, an average of 2 pedestrians per second enter the corridor and separated lanes from either side; the same conditions apply in the Layout C2 configuration, except that the pedestrians can only flow in one direction on each side. Pedestrians who enter the corridor have a 2% probability of suffering from COVID-19. The simulation stops after 80 s. Snapshots of simulations of these configurations are shown in Fig. 6.

There is a dramatic difference between the three configurations as R_{pd} increases; as shown in Fig. 7, T_{ac} and P_{ai} of the Layout C1 configuration are significantly lower than those of the other two configurations. In particular, the Layout C2 configuration leads to the longest time of contacts, the highest infection percentage, and the highest population density, as the columns dividing the corridor do not adequately separate the bidirectional flows of pedestrians and occupy space.

The Layout C1 configuration yields the best results, as its bidirectional flows of pedestrians are kept separate by the railings, thereby enabling faster flows of pedestrians than the other configurations. Both T_{ac} and P_{ai} in Layout C1 decline as the growth of R_{pd}, because these high-speed, separated bidirectional pedestrian flows reduce the possibility of transmission between pedestrians from a different direction, and thus transmission usually occurs between pedestrians travelling in the same direction.

Counterintuitively, both T_{ac} and P_{ai} in the Baseline C and the Layout C2 configurations are positively correlated (PCCs: 0.95) with R_{pd}, and unexpectedly peak at completely physical distance condition ($R_{pd} = 100\%$). On the one hand, pedestrians in a linear space follow the speed of pedestrians ahead in the line. Suppose the latter pedestrian has a higher walking speed, then he/she must slow down to match the former's slow speed, which reduces the average speed of the crowd as R_{pd} increases. Therefore, the lower evacuation efficiency increases exposure time and consequently results in higher P_{ai}. On the other hand, this counterintuitive finding is due to the space demands of physical distancing being opposed by the blockage caused by the high flow of pedestrians. The mean distance between pedestrians also accounts for this finding. Specifically, the mean distances between pedestrians in the Baseline C and Layout C2 configurations are 1.49 m and 1.44 m, respectively, at $R_{pd} = 0\%$, and decrease to 1.39 m and 1.35 m, respectively, at $R_{pd} = 100\%$. In contrast, the mean distance between pedestrians in the Layout C1 configuration is 1.45 m at $R_{pd} = 0\%$, and increases to 1.65 m at $R_{pd} = 100\%$. Consequently, these results indicate that high-density flows of pedestrians travelling in opposite directions must be separated by a barrier to prevent the transmission of infection [31].

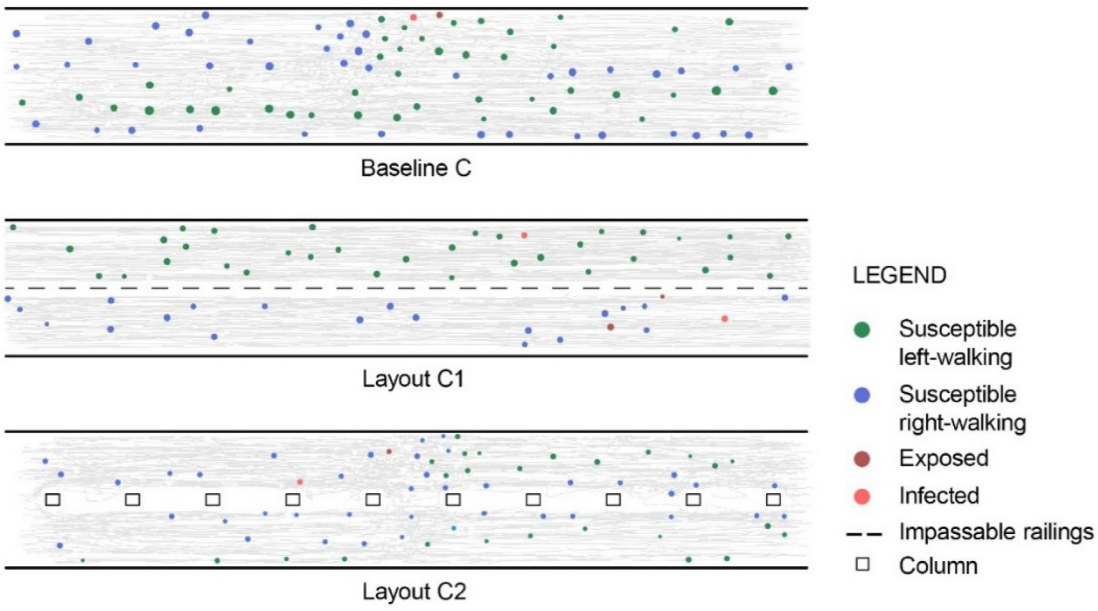

Fig. 6. Snapshot of three configurations of corridor simulations (simulation: 80 s; $R_{pd} = 100\%$).

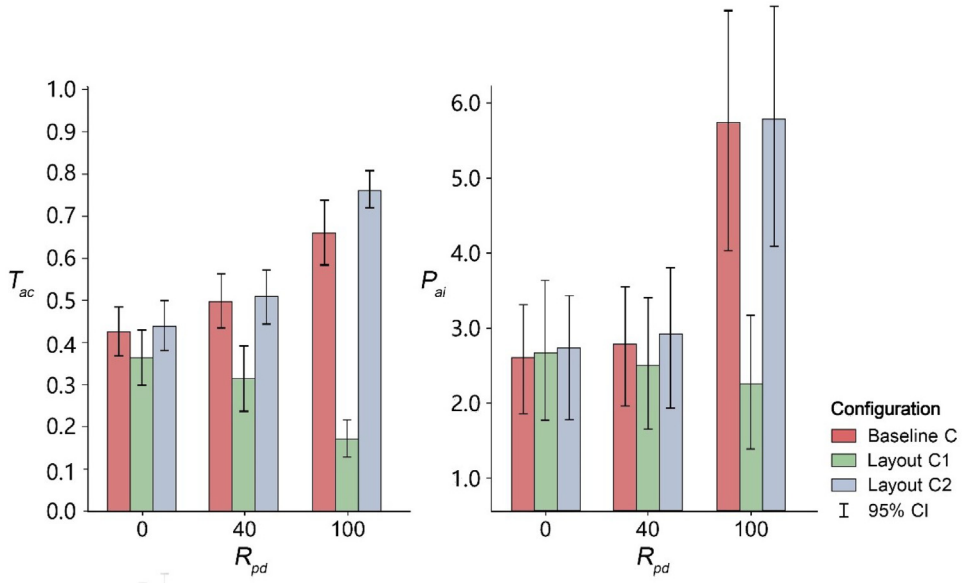

Fig. 7. Profiles of T_{ac} and P_{ai} for various corridor configurations and R_{pd}.

Fig. 8 shows that the variance between the three groups of data increases as R_{pd} increases. It can also be seen that some trajectories are clustered into several separate lanes, which was denoted 'lane formation' in a previous study [17]. Lane formation can increase the speed of pedestrians walking in opposite directions, resulting in the frequency and strength of pedestrian interactions decreasing, which mitigates the transmission of infection. The impassable railings in the Layout C1 configuration effectively separate opposing flows of pedestrians, and therefore this configuration has the best performance in all indicators. However, the occurrence of irregular motion can deform the lanes and thereby cause a blockage, which is denoted the 'freezing-by-heating' effect [50]. This effect is apparent in physical-distancing scenarios, as the corridor is too narrow to satisfy physical-distancing space requirements, which leads to pedestrians frequently varying their walking directions to avoid contact with each other. This can result in pedestrians blocking each other's passage, thereby causing local congestion (see the Baseline C and Layout C2 configuration results in Fig. 6) or whole-corridor blockage. Such blockage results in a gathering of pedestrians, thereby increasing the number of new infections.

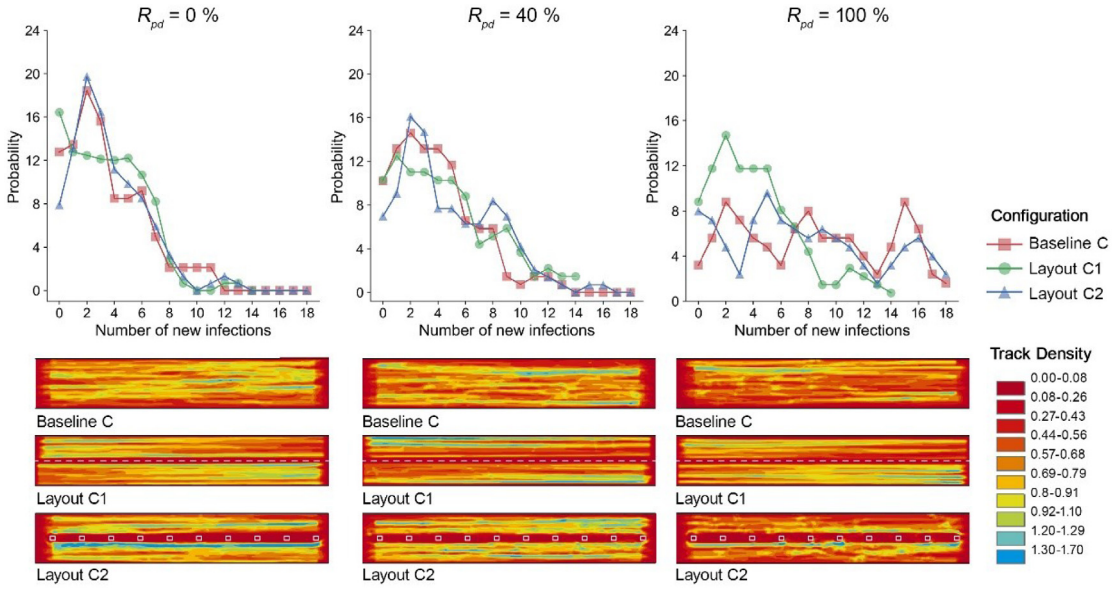

Fig. 8. Track densities and D_{ai} profiles of corridor simulations for various R_{pd}.

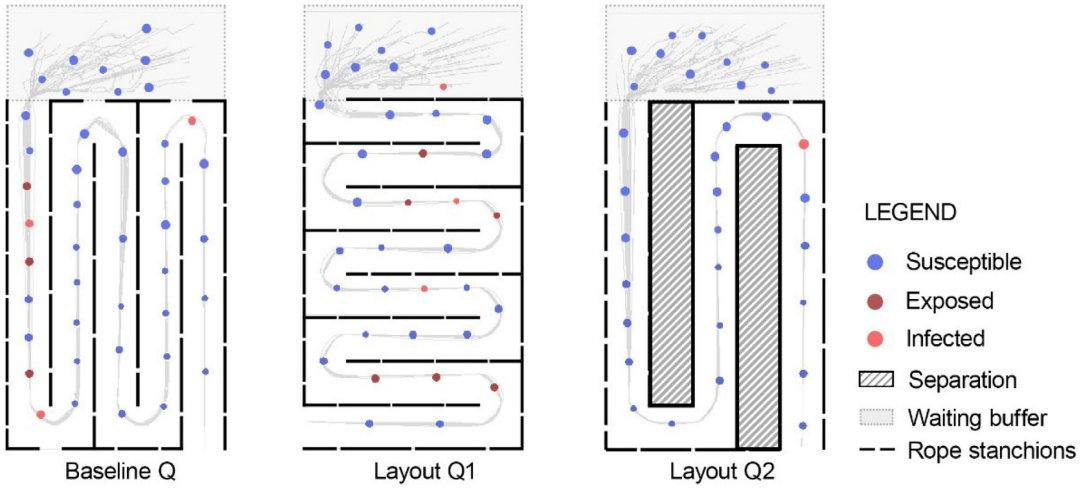

Fig. 9. Snapshot of three configurations of winding-queue simulations (simulation: 80 s; $R_{pd} = 100\%$).

4.5. Results of winding queue simulations

The establishment of winding queues of pedestrians is necessary for crowd management in many locations, such in airport security areas, or in ticket and security control areas in stadiums or at theme park attractions. Fig. 9 illustrates three winding-queue configurations in a 7.5 m $\times$ 12 m rectangular area with a 7.5 m $\times$ 3 m waiting buffer. Rope stanchions separate the queues, and the width of a single aisle is constant ($1.5m$), which means that S pedestrians may be within the infection-transmission radius of an I pedestrian if the latter is present in the same line as the former, or in an adjacent line [28]. The Baseline Q and Layout Q2 configurations are split vertically, while the Layout Q1 configuration is split horizontally. Separations are used in the Layout Q2 configuration to increase the contact distance between adjacent queues. Pedestrians flow at 1 pedestrian per second, enter the queue on the upper-left inlet from any possible position of the waiting buffer, and walk towards the bottom exit. Pedestrians may walk side-by-side in the waiting buffer, yet most pedestrians eventually merge into a single queue in the process of entering the queue under physical-distancing conditions. The stop conditions and infection probability are the same as in the corridor simulations.

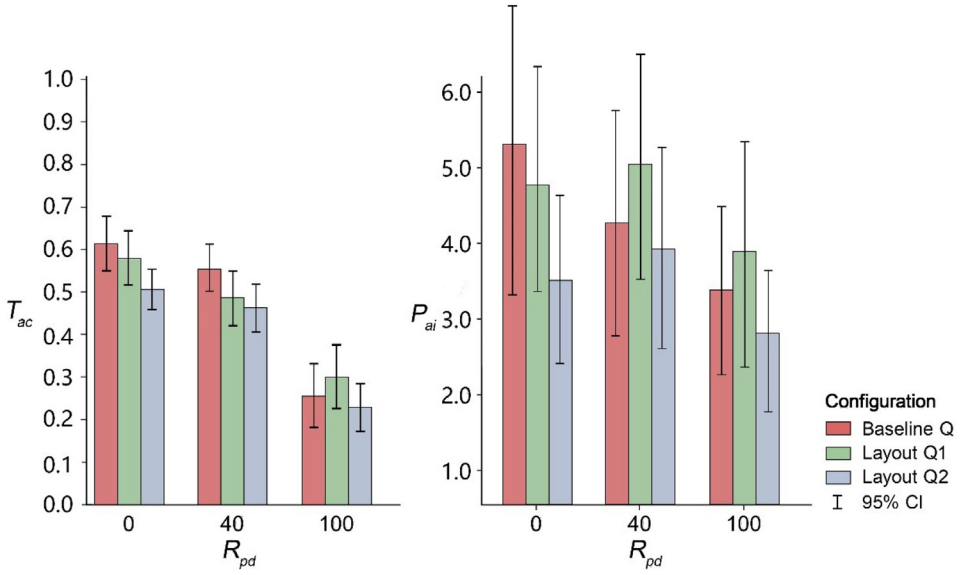

Fig. 10. Profiles of T_{ac} and P_{ai} for various winding-queue configurations and R_{pd}.

As shown in Fig. 10, pedestrians in the Baseline Q and Layout Q1 configurations are more likely to be infected than those in the Layout Q2 configuration; this is because the transmission radius is larger than the width of the aisles in the former two configurations, which may lead to cross-aisle contact between pedestrians, and thus transmission of infection. The Layout Q2 configuration is the best, because the separation between aisles prevents the transmission of infection between pedestrians in adjacent aisles.

The Layout Q2 configuration is worse than the Baseline Q configuration under physical distancing condition, because in the former the transmission radius is large enough that infected pedestrians can contact more pedestrians at corners than across aisles. Moreover, short aisles lead to congestion around corners, as pedestrians must often reduce their walking speed to turn at corners [28]. Therefore, the evacuation efficiency of the Layout Q1 is lower than that of the Baseline Q. In contrast, pedestrians in long aisles have more time to adjust their distance from the pedestrian in front of them, and thus a more stable formation and lower average density are maintained. As a result, overtaking behaviours caused by the various desired speeds of pedestrians occur more frequently on a longer aisle than a short one. Such frequent interaction between pedestrians lead to a longer T_{ac}, thus T_{ac} in the Baseline Q is higher than that in the Layout Q1 at $R_{pd} = 0\%$ and 40%.

Furthermore, there is a downward trend of P_{ai} as R_{pd} grows in the Baseline Q, but no similar relationship is detected in the Layout Q1 and Q2. Specifically, although P_{ai} in Baseline Q is the highest of three configurations under non-physical distancing walking environment ($R_{pd} = 0\%$) because of a longer T_{ac}, the P_{ai} of Layout Q1 remains the highest at $R_{pd} = 40\%$ and 100%. Such a fact indicates that evacuation efficiency plays a more critical role than T_{ac} under a physical distancing condition ($R_{pd} > 0\%$).

Counterintuitively, a high infection-transmission probability is presented at $R_{pd} = 40\%$ and 100% of Layout Q1 and Layout Q2. It is because when pedestrians who ignore physical distance overtake those who obey, the latter have to slow down and get out of the way. Also, pedestrians may get closer to the overtaken pedestrian during overtaking manoeuvres, notably increasing the infection rate if another pedestrian is infected. Such a fact leads to a lower mean speed of the crowd and a higher crowd density, thus resulting in a higher infection percentage at $R_{pd} = 40\%$.

Fig. 11 shows that the probability of infection transmission decreases exponentially as the number of new infections increases. The Layout Q2 configuration results in relatively high probabilities of a low number of infections and low probabilities of a high number of infections, whereas the converse is true for the other two configurations, especially the Layout Q1 configuration. The probability of infection transmission to zero pedestrians increases as R_{pd} increases. There are a maximum of 17 newly infected pedestrians in the Baseline Q configuration, but a maximum of 12 newly infected pedestrians in the Layout Q2 configuration; this greater than 33% reduction is attributable to the fact that the Layout Q2 configuration has fewer corners and neighbouring aisles than the Baseline Q configuration. The trajectory density also decreases as R_{pd} increases, which decreases the transmission of infection.

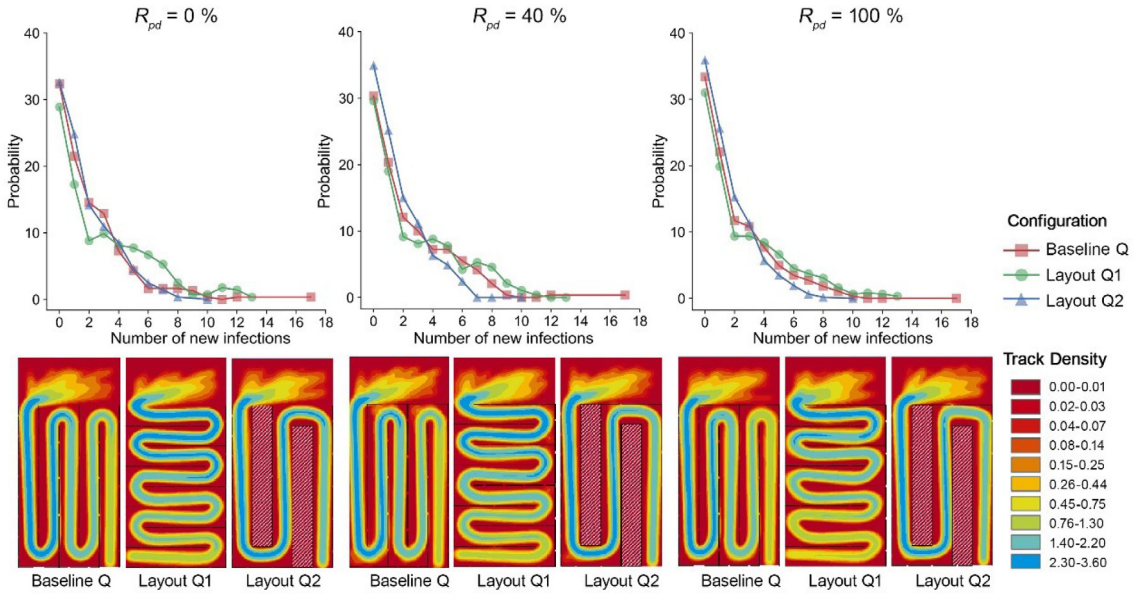

Fig. 11. Track densities and D_{ai} profiles of winding-queue simulations for various R_{pd}.

5. Discussion

People have responded to the global pandemic of COVID-19 by altering the way they adapt to spaces [6]. We identify strategies that can reduce the transmission of SARS-COV-2 by developing the PDM, a model that considers the effects of physical distancing. This allows us to examine the relationship between infection transmission and two spatial measures that may prevent such transmission: physical distancing and space design. In our systematic simulation-based approach, trajectories and contact data between I and S pedestrians are determined using a dynamic simulation of physical distancing, then utilised to estimate the number of new infections in various space configurations and at various values of R_{pd}.

The PDM has more features than its predecessor, the SFM, such as parameters related to the infection-prevention sphere in response to the space requirements of physical distancing, and a new computation that involves calculating the force of the nearest pedestrian and the force of other pedestrians separately. The results of PDM simulations are very similar to the results of SFM simulations for $R_{pd} = 0\%$. However, as R_{pd} increases, the PDM simulates richer interactions than the SFM, including interactions between pedestrians who do not observe physical distancing, between pedestrians who do observe physical distancing, and between these two types of pedestrians.

Counterintuitively, higher R_{pd} values do not necessarily result in fewer infections, as indicated in Figs. 7 and 10; the most critical factors that affect infection transmission are limitations of space and diversity of pedestrian walking speed. During evacuation scenarios when R_{pd} is less than 100%, frequent, robust interactions occur between pedestrians who do not observe physical distancing and those who do, particularly during overtaking manoeuvres in a narrow space. In addition, those who observe physical distancing must sometimes slow down and give way to those who do not, which reduces the mean speed and increases the pedestrian density. Such interactions increase the close contact between non-infected and infected pedestrians and reduce the walking efficiency, which increases the infection percentage. Additionally, blockages caused by the 'freezing-by-heating' effect is another reason to explains the high infection-transmission probability, which is discussed detailly below.

5.1. Observation of collective phenomena

Some collective phenomena observed in the SFM, such as arching, lane formation, and 'freezing-by-heating', also occur in the PDM, but with differences. For example, uneven density occurs during arching and there are higher frequencies of the 'freezing-by-heating' effect, both of which are due to more demand for space under physical-distancing conditions. These novel manifestations of collective phenomena in the PDM significantly affect infection transmission. Physical distance is greatly affected by space, and thus space design must comprehensively consider pedestrian self-organisation, in addition to the space demands of physical distancing during pedestrian movement. Limiting the flow of pedestrians can prevent the 'freezing-by-heating' effect, and scenario simulations in this study also indicate that correctly planning the layout of a space is vital to limiting the transmission of SARS-CoV-2 under physical-distancing conditions. Thus, the evaluation and optimisation of space configurations is paramount.

5.2. Recommendations for space design

In this paper we demonstrate our approach for space design by examining three typical public spaces in various configurations. We find that increasing the numbers and widths of entries into public spaces are effective strategies for decreasing the transmission of infection in a crowded, closed room (see Fig. 4). Additionally, if physically distancing pedestrians are moving in opposite directions in a linear corridor, blockages of pedestrians may occur, leading to large-scale infection transmission. Thus, barriers should be installed between flows of pedestrians moving in opposite directions. A continuous interface performs better than a permeable interface in this regard, and thus railings in the middle of a corridor can prevent the irregular motion of pedestrians, effectively reducing the numbers of contacts and suppressing the spread of infection (see Fig. 7). Furthermore, our simulations show that decreasing the number of corners in a winding queue reduces queuing pedestrians' contact frequency and direction-change deceleration, and thus decreases the spread of infection. Long aisles are therefore better than short aisles under physical-distancing conditions, as the former allow queuing pedestrians to better adjust their distance from others, and thus maintain a stable formation and low average density, reducing their exposure to infected pedestrians. Separations between adjacent aisles are another effective configuration, as they reduce cross-aisle contact and thus infection transmission (see Fig. 10).

6. Conclusion

The practice of physical distancing and the establishment of correct space layouts are effective measures for preventing and mitigating the transmission of SARS-CoV-2. Physical distancing is greatly influenced by space organisation, such that physical distancing in a small and crowded space can be counterproductive. Thus, an effective combination of these two spatial prevention measures is needed to minimise viral transmission.

To this end, we systematically develop a simulation-based approach that combines physical-distancing pedestrian dynamics with an infection judgement framework to estimate the effect of spatial configuration management on the fine-scale spread of infection. This approach has three advantages. First, it simulates the evacuation dynamics under physical-distancing conditions by describing the advancement and adjustment behaviours of physical-distancing pedestrians, thereby simulating the exploration process of pedestrians in a continuous action space. Second, it evaluates the infection-transmission probability in different spatial forms. This reveals that decreases in the effects of physical distancing occur due the conflict between limited interior spaces and the demands of physical distancing for larger spaces, and due to the relative relationship between crowd density and evacuation efficiency. Phenomena such as 'freezing-by-heating' and uneven arching reduce evacuation efficiency, and may cause large-scale infection. Therefore, conflicting spatial availability and spatial demands should be alleviated by widening the exits of closed rooms and installing separation barriers in corridors, and the relationship between density and efficiency should be balanced by increasing the number of exits from closed rooms. Furthermore, the installation of separations between aisles can block the transmission of infection between queuing pedestrians in opposite aisles traversed by the same winding queue. Third, this approach has enormous application potential for other infectious-disease transmission and space assessments. The parameters in the model can be modified to generate a rich and tailored application scenario, allowing the pedestrian dynamics model to simulate the physical distancing of crowds in larger spaces, such as museums, railway stations, airports, and schools. The infection-transmission model can also be tailored to allow examination of the transmission dynamics of similar infectious respiratory diseases, by modifying the parameters of transmission mechanisms.

Nevertheless, despite extensive efforts to ensure the validity of our conclusions, there are some limitations to the parameter calibration and model verification. First, although we vary the model parameters over a vast design space and they reflect real-life physically distanced pedestrian passage, it remains to be determined that these parameters are optimal; this will be explored in future work. Second, although a comparison between simulation results and real-world data is needed to confirm the external validity of our findings, this is beyond the scope of the current paper. However, this remains a crucial aspect to explore. Thus, in future work, we will use video-tracking data of volunteer pedestrians to calibrate the model, and determine improvements in its goodness-of-fit in terms of a specified interaction force. Finally, we assume that the presentation of SARS-CoV-2 particles is centred on the source of infection and spreads to all sides, and that the particle distribution is consistent. This is a simplification, and may deviate from reality; thus, expanded calculations should be used to adjust the infection model to account for the range of exhaled particles and the range of a pedestrian's inhalation.

New design guidelines for physical distancing will affect the organisation of public spaces in the future. This study demonstrates how pedestrian dynamics can be used to evaluate the effectiveness of public-space layout design, and facilitate physical distancing, to prevent the transmission of SARS-CoV-2. Specifically, by dynamically depicting the trajectory of pedestrians in space and assessing the transmission of infection between pedestrians, dynamic simulations of viral transmission are achieved. Our research is therefore an effective illustration of how mathematical modelling could guide space management and design for public health optimisation.

CRediT authorship contribution statement

Tianyi Xiao: Conceptualisation, Methodology, Software, Validation, Formal analysis, Writing – original draft, Writing – review & editing, Visualisation, Investigation, Data curation. **Tong Mu:** Writing – original draft, Writing – review & editing. **Sunle Shen:** Software, Formal analysis, Investigation, Data curation, Visualisation. **Yiming Song:** Writing – review & editing, Visualisation. **Shufan Yang:** Writing – review & editing. **Jie He:** Conceptualisation, Writing – review & editing, Project administration, Funding acquisition, Supervision.

Declaration of competing interest

The authors declare that they have no known competing financial interests or personal relationships that could have appeared to influence the work reported in this paper.

Acknowledgements

This research was supported by Open Projects Fund of Key Laboratory of Ecology and Energy-Saving Study of Dense Habitat (Tongji University), Ministry of Education, China, 2020–2021, for Physical-Distancing-Based Microscopic Traffic Simulation and Path Planning of Students: A Case Study of Tianjin (Grant No. 2020030101).

References

[1] World Health Organization, WHO coronavirus (COVID-19) dashboard, 2021, Retrieved from https://covid19.who.int/.
[2] S. Zhang, M. Diao, W. Yu, L. Pei, Z. Lin, D. Chen, Estimation of the reproductive number of novel coronavirus (COVID-19) and the probable outbreak size on the diamond princess cruise ship: A data-driven analysis, Int. J. Infect. Dis. 93 (2020) 201–204.
[3] M. Shen, Z. Peng, Y. Guo, L. Rong, Y. Li, Y. Xiao, G. Zhuang, L. Zhang, Assessing the effects of metropolitan-wide quarantine on the spread of COVID-19 in public space and households, Int. J. Infect. Dis. 96 (2020) 503–505.
[4] M. Chinazzi, J.T. Davis, M. Ajelli, C. Gioannini, M. Litvinova, S. Merler, A.P. y Piontti, K. Mu, L. Rossi, K. Sun, The effect of travel restrictions on the spread of the novel coronavirus (COVID-19) outbreak, Science 368 (2020) (2019) 395–400.
[5] N.A.B. Abdul Nasir, A.S. Hassan, F. Khozaei, M.H.B. Abdul Nasir, Investigation of spatial configuration management on social distancing of recreational clubhouse for COVID-19 in penang, Malaysia, Int. J. Build. Pathol. Adapt. (2020).
[6] R.F. Hunter, L. Garcia, T.H. de Sa, B. Zapata-Diomedi, C. Millett, J. Woodcock, A.S. Pentland, E. Moro, Effect of COVID-19 response policies on walking behavior in US cities, Nature Commun. 12 (2021).
[7] W.O. Kermack, À.G. Mckendrick, A contribution to the mathematical theory of epidemics, Proc. R. Soc. A: Math. Phys. Eng. Sci. 115 (1927) 700–721.
[8] T. Britton, Stochastic epidemic models: A survey, Math. Biosci. 225 (2010) 24–35.
[9] J. Gani, Stochastic epidemic models and their statistical analysis, J. Amer. Statist. Assoc. 97 (2002) 659.
[10] D. Balcan, V. Colizza, B. Goncalves, H. Hu, J.J. Ramasco, A. Vespignani, Multiscale mobility networks and the spatial spreading of infectious diseases, Proc. Natl. Acad. Sci. USA 106 (2009) 21484–21489.
[11] L.A. Rvachev, I. Longini, A mathematical model for the global spread of influenza, Bellman Prize Math. Biosci. 75 (1985) 3–22.
[12] M. Chang, R. Kahn, Y. Li, C. Lee, C.O. Buckee, H. Chang, Variation in human mobility and its impact on the risk of future covid-19 outbreaks in taiwan, Vol. 21, BMC Public Health, 2021.
[13] S. Okazaki, A study of pedestrian movement in architectural space, part 1: Pedestrian movement by the application on of magnetic models, Trans. AIJ 283 (1979) 111–119.
[14] M. Fukui, Y. Ishibashi, Jamming transition in cellular automaton models for pedestrians on passageway, J. Phys. Soc. Japan 68 (1999) 3738–3739.
[15] D. Helbing, Molnar, Social force model for pedestrian dynamics, Phys. Rev. E 51 (1995) 4282–4286.
[16] D. Helbing, L. Buzna, A. Johansson, T. Werner, Self-organized pedestrian crowd dynamics: Experiments, simulations, and design solutions, Transp. Sci. 39 (2005) 1–24.
[17] D. Helbing, A. Johansson, Pedestrian, crowd, and evacuation dynamics, in: Encyclopedia of Complexity and Systems Science, 2009.
[18] N. Cao, Z. Qu, Y. Chen, L. Zhao, X. Song, Q. Bai, Destination and route choice models for bidirectional pedestrian flow based on the social force model, IET Intell. Trans. Syst. 11 (2017) 537–545.
[19] Y. Suma, D. Yanagisawa, K. Nishinari, Anticipation effect in pedestrian dynamics: Modeling and experiments, Physica A 391 (2012) 248–263.
[20] F. Farina, D. Fontanelli, A. Garullil, A. Giannitrapanil, D. Prattichizzol, Ieee, when helbing meets laumond: The headed social force model, in: 55th IEEE Conference on Decision and Control, CDC, Las Vegas, NV, 2016, pp. 3548–3553.
[21] D.R. Parisi, M. Gilman, H. Moldovan, A modification of the social force model can reproduce experimental data of pedestrian flows in normal conditions, Physica A 388 (2009) 3600–3608.
[22] Y. Gao, P. Luh, H. Zhang, T. Chen, A modified social force model considering relative velocity of pedestrians, in: 2013 IEEE International Conference on Automation Science and Engineering, CASE, 2013, pp. 747-751.
[23] D.R. Parisi, G.A. Patterson, L. Pagni, A. Osimani, T. Bacigalupo, J. Godfrid, F.M. Bergagna, M.R. Brizi, P. Momesso, F.L. Gomez, Social distance characterization by means of pedestrian simulation, 2020, arXiv preprint arXiv:2009.04019.
[24] I. Echeverría-Huarte, A. Garcimartín, R.C. Hidalgo, C. Martín-Gómez, I. Zuriguel, Estimating density limits for walking pedestrians keeping a safe interpersonal distancing, Sci. Rep. 11 (2021) 1534.
[25] C.A. Pouw, F. Toschi, F. van Schadewijk, A. Corbetta, Monitoring physical distancing for crowd management: Real-time trajectory and group analysis, PLoS One 15 (2020) e0240963.
[26] C.M. Mayr, G. Köster, Social distancing with the optimal steps model, 2020, arXiv preprint arXiv:2007.01634.
[27] S. Namilae, P. Derjany, A. Mubayi, M. Scotch, A. Srinivasan, Multiscale model for pedestrian and infection dynamics during air travel, Phys. Rev. E 95 (2017).
[28] P. Derjany, S. Namilae, D. Liu, A. Srinivasan, Multiscale model for the optimal design of pedestrian queues to mitigate infectious disease spread, PLoS One 15 (2020).
[29] H. Sun, X. Liu, X. Xu, Y. Wu, Analysis of COVID-19 spreading and prevention strategy in schools based on continuous infection model, Acta Phys. Sin. 69 (2020).

[30] A.R. Tilley, The Measure of Man and Woman: Human Factors in Design, Wiley, New York, 2002.
[31] D. Helbing, P. Molnár, I. Farkas, K. Bolay, Self-organizing pedestrian movement, Environ. Plan. B: Plann. Des. 28 (2001) 361–383.
[32] R. Knoblauch, M. Pietrucha, M. Nitzburg, Field studies of pedestrian walking speed and start-up time, Transp. Res. Rec. 1538 (1996) 27–38.
[33] China State Bureau of Technical Supervision, Human dimensions of Chinese adults, (GB/T 10000-1988).
[34] D. Helbing, I. Farkas, T. Vicsek, Simulating dynamical features of escape panic, Nature 407 (2000) 487–490.
[35] Centers for Disease Control and Prevention, Social distancing: Keep a safe distance to slow the spread, 2021, Retrieved from https://www.cdc.gov/coronavirus/2019-ncov/prevent-getting-sick/social-distancing.html.
[36] Queensland Government, How to protect yourself and others—coronavirus (COVID-19), 2021, Retrieved from https://www.qld.gov.au/health/conditions/health-alerts/coronavirus-covid-19/protect-yourself-others/coronavirus-prevention.
[37] A. Agrawal, R. Bhardwaj, Probability of COVID-19 infection by cough of a normal person and a super-spreader, Phys. Fluids 33 (2021).
[38] D. Helbing, A. Johansson, H.Z. Al-Abideen, Dynamics of crowd disasters: An empirical study, Phys. Rev. E 75 (2007).
[39] A. Agrawal, A.K. Prasad, Integral solution for the mean flow profiles of turbulent jets, plumes, and wakes, J. Fluids Eng.-Trans. Asme 125 (2003) 813–822.
[40] S.N. Rudnick, D.K. Milton, Risk of indoor airborne infection transmission estimated from carbon dioxide concentration, Indoor Air 13 (2003) 237–245.
[41] A. Moskal, L. Gradon, Temporary and spatial deposition of aerosol particles in the upper human airways during breathing cycle, J. Aerosol Sci. 33 (2002) 1525–1539.
[42] N.H. Leung, D.K. Chu, E.Y. Shiu, K.-H. Chan, J.J. McDevitt, B.J. Hau, H.-L. Yen, Y. Li, D.K. Ip, J.M. Peiris, Respiratory virus shedding in exhaled breath and efficacy of face masks, Nat. Med. 26 (2020) 676–680.
[43] X. He, E.H. Lau, P. Wu, X. Deng, J. Wang, X. Hao, Y.C. Lau, J.Y. Wong, Y. Guan, X. Tan, Temporal dynamics in viral shedding and transmissibility of COVID-19, Nat. Med. 26 (2020) 672–675.
[44] Y. Liu, Z. Ning, Y. Chen, M. Guo, Y. Liu, N.K. Gali, L. Sun, Y. Duan, J. Cai, D. Westerdahl, Aerodynamic analysis of SARS-CoV-2 in two wuhan hospitals, Nature 582 (2020) 557–560.
[45] J.A. Lednicky, M. Lauzard, Z.H. Fan, A. Jutla, T.B. Tilly, M. Gangwar, M. Usmani, S.N. Shankar, K. Mohamed, A. Eiguren-Fernandez, Viable SARS-CoV-2 in the air of a hospital room with COVID-19 patients, Int. J. Infect. Dis. 100 (2020) 476–482.
[46] K.A. Prather, C.C. Wang, R.T. Schooley, Reducing transmission of SARS-CoV-2, Science 368 (2020) 1422–1424.
[47] J.H. Sullivan, M. Warkentin, L. Wallace, So many ways for assessing outliers: What really works and does it matter? J. Bus. Res. 132 (2021) 530–543.
[48] Environmental Systems Research Institute, Inc., How kernel density works, 2016, Retrieved from https://desktop.arcgis.com/en/arcmap/10.3/tools/spatial-analyst-toolbox/how-kernel-density-works.htm.
[49] Y. Han, H. Liu, Modified social force model based on information transmission toward crowd evacuation simulation, Physica A 469 (2017) 499–509.
[50] D. Helbing, I.J. Farkas, T. Vicsek, Freezing by heating in a driven mesoscopic system, Phys. Rev. Lett. 84 (2000) 1240–1243.
[51] D. Helbing, A mathematical model for the behavior of pedestrians, Syst. Res. Behav. Sci. 36 (1991) 298–310.